Using AI

- How to use AI

The template below is to be used in your report for your report and code submission

Permitted Uses: I acknowledge that I am permitted to use AI tools for research, brainstorming, concept clarification, debugging assistance, and writing support, but NOT for directly answering assignment questions or generating my final code solutions.

Acknowledgement:
☐ I have not used any AI tools or technologies to prepare this assessment.

OR

☑ I acknowledge the use of [AI tool name and link] to assist with [select appropriate activities from the list below]:
a) Background research and concept exploration
b) Brainstorming design approaches
c) Understanding space engineering principles
d) Debugging code logic (without generating final solutions)
e) Writing assistance (grammar, structure, clarity)
f) Literature review support
g) Other: _____

How I Used the Output: I used the AI output to [describe specific activities, such as]:
a) Gain foundational understanding before developing my own analysis
b) Generate initial ideas that I then researched and developed independently
c) Check my understanding of concepts before applying them to my solutions
d) Improve the clarity and structure of my written explanations
e) [Other appropriate uses]

Final Work Confirmation: I confirm that:
a) All mathematical calculations and engineering analyses are my own work
b) All code was written by me (though I may have used AI for debugging assistance)
c) All final answers and conclusions are based on my own reasoning and application of engineering principles
d) Any AI-generated content was used only as a starting point and was substantially modified and verified through my own work

Constellation Design and Orbit Determination for Satellite Emergency Communication Network

Noah West, *530494928*

I. Question 1

A. Introduction

Satellites currently provide a range of critical capabilities to Australian emergency services [1]. During bushfires, firefighters use satellites for imaging the fire, predicting weather, finding water, locating distress beacons, and remote communication. Additionally, many remote areas of Australia don't have mobile data or radio coverage. By improving emergency communication via satellite networks, harm can be reduced or prevented.

We have been tasked with designing a satellite communications network which can provide persistent, low latency (less than 25 ms one-way) communication to the blue mountains. Communication can only occur when there is a direct line of sight from the observer to at least one satellite. On flat terrain, a satellite only needs to be above the horizon, but in the Blue Mountains local topography blocks low-elevation views. We therefore require at least one satellite above 30° elevation—about 5° higher than the Starlink minimum [2]. At this angle, even an observer at the base of a 300 m cliff can maintain line-of-sight if 500 m from the face; closer than that, it is reasonable to wait briefly or move to regain visibility.

Below are our requirements,

- R1 A satellite must be visible by any ground level observer around (33.610000 S, 150.464444 E) at all times
- R2 A satellite must be above 30 degrees elevation more 95 % of the time.
- R3 Intervals of time where 30 degrees of elevation isn't met must be less than 1 minutes long.
- R4 A satellite must be above 25 degrees elevation 100% of the time.
- R5 The one way latency must be below 25 ms

B. Method

Designing the orbits for the satellites begins with designing geometric constraints for the problem. Figure 1 illustrates where satellites can be for line of sight communication to occur with the blue mountains. This region is a circle sector revolved about the zenith at the Blue Mountains, which does not intersect the equatorial plane. In this section, we develop a method of finding the orbit constellation that spends the most time in this sector, with the least number of satellites.

To find the duration of visibility of a satellite throughout a full orbit, the orbit needs to be simulated in the Earth Centred Inertial (ECI) reference frame, then the ground observer needs to be found in the ECI frame. Then, the relative vector between the satellite and ground observer needs to be found in the Topocentric horizon coordinate system, before begin converted to azimuth, elevation and range.

1) Propagating Satellites

For a given set of Keplerian orbital parameters, we can determine an initial state vector, from which we can generate the corresponding orbit path in the ECI frame by numerically integrating the satellite's initial state. The state vector $\boldsymbol{x}$ of the satellite is propagated with a RK45 integrator, using the two-body equation with J2 perturbations due to Earth's oblateness.

$$\dot{\boldsymbol{x}}_{sat} = \begin{bmatrix} \dot{r}_x \\ r_y \\ r_z \\ v_x \\ v_y \\ v_z \end{bmatrix} = \begin{bmatrix} v_x \\ v_y \\ v_z \\ \boldsymbol{a_{tb}} + \boldsymbol{a_{j2}} \end{bmatrix} \tag{1}$$

Where the two body acceleration$\boldsymbol{a_{tb}}$ is given by

$$\boldsymbol{a_{tb}} = \begin{bmatrix} -\mu r_x/r^3 \\ -\mu r_y/r^3 \\ -\mu r_z/r^3 \end{bmatrix} \tag{2}$$

where μ is the Earth's gravitational constant. The acceleration due to J2 perturbations $\boldsymbol{a_{j2}}$ is given by,

$$\boldsymbol{a_{j2}} = -\frac{3J_2\mu R_e^2}{2r^5} \begin{bmatrix} r_x(1-5r_z^2/r^2) \\ r_y(1-5r_z^2/r^2) \\ r_z(3-5r_z^2/r^2) \end{bmatrix} \tag{3}$$

where R_e is the equatorial radius of the Earth, and J2 is the first gravitation zonal harmonic of Earth.

2) Converting LLA to ECI

The observer's coordinates in Latitude, Longitude and Altitude (LLA), are converted to ECI with the following process.

The oblateness of the Earth is considered with,

$$f = \frac{R_e - R_p}{R_e} = 0.003352813$$

where R_p, f are the polar radius of Earth, and the flattening of Earth respectively. The distance from C' to O, R_ϕ, (depicted in Appendix Figure 19) is given by,

$$R_\phi = \frac{R_e}{\sqrt{1-(2f-f^2)\sin^2\phi}}$$

where ϕ is the geodetic latitude provided (-33.61).

The distance R_c from C' to the station if the station is H meters above point O, and the distance R_s from the station

to where OC' intersection the equatorial plane are each given by,

$$R_c = R_\phi + H \qquad R_s = (1-f)^2 R_\phi + H$$

Lastly, the position vector $\boldsymbol{r}_{ECEF}$ in the Earth Centred, Earth Fixed (ECEF) reference frame is given by,

$$\boldsymbol{R}_{ECEF} = R_c \cos\phi \cos\theta \hat{\boldsymbol{I}} + R_c \cos\phi \sin\theta \hat{\boldsymbol{J}} + R_s \sin\phi \hat{\boldsymbol{K}}$$

where θ is the longitude. To convert to ECI, we use a rotation matrix $\boldsymbol{Q}_{ECEF \to ECI}$

$$= \begin{bmatrix} \cos\theta_{G0} & -\sin\theta_{G0} & 0 \\ \sin\theta_{G0} & \cos\theta_{G0} & 0 \\ 0 & 0 & 1 \end{bmatrix} \tag{4}$$

where θ_{G0} is the Greenwich Median Sidereal Time (GMST).

Julian day can be calculated from the current date Y/M/D and Universal time UT in hours,

$$J_D = 367Y - [\frac{7[y + (\frac{M+9}{12})]}{4}] + [\frac{275M}{9}] + D + 1721013.5 + \frac{UT}{24}$$

From Julian date, GMST θ_{G0} is calculated as,

$$\theta_{G0} = 100.46062 + 36001 T_0 + 0.000387933 T_0^2 + 2.583(10^-8) T_0^3$$

Where T_0 is time in Julian centuries, which is calculated with,

$$T_0 = \frac{J_0 - 2451545}{36525}$$

This needs to be done for each time step.

3) Ground Tracks

To produce the ground tracks, the inverse of the LLA to ECI transformation process is performed at each time step.

$$\boldsymbol{R}_{ECEF} = \boldsymbol{Q}^T_{ECEF \to ECI}\ \boldsymbol{R}_{ECI}$$

Then convert to geodetic latitude and longitude ϕ, θ with,

$$\phi = \sin^{-1}(\frac{R_{ECEF,z}}{|\boldsymbol{R}_{ECEF}|})$$

$$\theta = \text{atan2}(\frac{R_{ECEF,x}}{R_{ECEI,y}})$$

4) Converting to Azimuth and Elevation

With both the observer and the satellite in the ECI frame, we can firstly plot them together (see Figure 3 in Results). We can figure out the coordinates of the satellite in an East North Up (ENU) frame $\boldsymbol{\rho}_{ENU}$, with the relative vector between the observer and the satellite $\boldsymbol{\rho}_{ECI}$ and the transformation matrix $\boldsymbol{Q}_{Xx}$ defined by geodetic latitude and Local Sidereal Time LST (ϕ, θ_{LST}),

$$\boldsymbol{\rho}_{ECI} = \boldsymbol{r}_{sat,ECI} - \boldsymbol{R}_{observer,ECI}$$

$$\boldsymbol{Q}_{Xx} = \begin{bmatrix} -\sin\theta_{LST} & \cos\theta_{LST} & 0 \\ -\sin\phi\cos\theta_{LST} & -\sin\phi\sin\theta_{LST} & \cos\phi \\ \cos\phi\cos\theta_{LST} & \cos\phi\sin\theta_{LST} & \sin\phi \end{bmatrix} \tag{5}$$

$$\boldsymbol{\rho}_{ENU} = \boldsymbol{Q}_{Xx}\ \boldsymbol{\rho}_{ECI} \tag{6}$$

Azimuth A and elevation α in ENU can be calculated with,

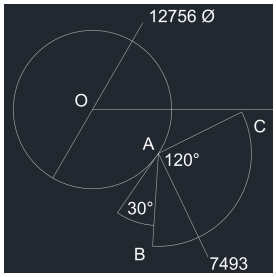

Figure 1: Illustration of field of view of Blue Mountains accounting for minimum elevation angle and maximum communication delay. A satellite needs to be in sector ABC to be visible. The circle with centre O is a cross section of the Earth, with the North Pole at the top and the Blue Mountains at A

$$A = \arctan 2(\frac{\rho_{EAST}}{\rho_{NORTH}}) \tag{7}$$

$$\alpha = \sin^{-1}\frac{\rho_{UP}}{|\boldsymbol{\rho}_{ENU}|} \tag{8}$$

Our constellation of satellites meets requirements when $\alpha > 30$ for at least 1 satellite 95 percent of the time, and $\alpha > 20$ all the time, as well as $|\boldsymbol{r_{s,o}}| < 7498$ km. This can be verified by performing the transformation at each time step using the numerically generated state array.

5) Designing the constellation

To have constant coverage of the Blue Mountains, we require a constellation of Satellites. In the interest of cost, this should be done with a minimum number of satellites. Additionally, communication windows should be as long as possible, to avoid frequent switching of communication paths, and revisit time should be less than a day to allow for diagnostic checks for each satellite.

6) Searching harmonic orbits

Orbits with periods that are an integer times faster than one sidereal day are explored as potential candidates for our satellites. For Geosynchronous and Molniya orbits (see Appendix Figure 20), only a small part of the orbit will be within communicating distance with the Earth. Fortunately, we can position the orbit such that the perigee is always above the Blue Mountains.

A grid search was conducted for orbits with orbit period : Earth period ratios of $1:n$ for $n \in \{1,2,3,4,5,6,7,8,9,10\}$.

Grid search explored a variety of eccentricities and true anomalies for each of the orbit harmonics. Inclination angle (i) was set to align with the Blue Mountains, the semi-major axis (a) was determined with Kepler's 3rd Law. The Argument Of Perigee (AOP/(ω)) was 270 (so the perigee is at the bottom of the ground track). Right Ascension of the Ascending Node (RAAN/Ω) was 0.

7) Searching non-harmonic circular orbits

non-harmonic circular orbits with semi-major axis between 11543 and the maximum radius of communication given by,

$$a = R_\oplus + 7499 = 13877 \text{ km},$$

were explored too.

$R_\oplus$ is Earth's mean radius. A larger altitude allows for a greater portion of the orbit to be in the sector of visibility. A grid search was performed with the following parameters.

$$11{,}543 \text{ km} \leq a \leq 13{,}877 \text{ km},$$

with orbital elements defined as: $e = 0$, $\theta_a = 189°$, $\Omega = 0°$, $\omega = 270°$.

Inclination (i) and semi-major axis (a) were varied to evaluate visibility performance.

8) Calculating Period

The orbital period can be calculated by rearranging Kepler's Third Law,

$$T = \sqrt{\frac{4\pi^2 a^3}{\mu}}$$

C. Results and Discussion

1) Harmonic orbits

The geosynchronous and Molniya orbit options are impractical, because the grid search (depicted in Figure 21) found that the maximum portion of time spent for a satellite in this window is 2.26%. This means long revisit time, short communication windows and low global coverage per satellite.

Table I: Harmonic orbital periods and visibility percentages

Period Earth:Sat	Semi-major axis [km]	Visible Percentage [%]
1:3	20397	3.20
1:4	16763	4.20
1:5	14446	5.56
1:6	12793	7.87
1:7	11543	9.03
1:8	10560	7.64
1:9	9763	5.90
1:10	9101	5.20

Table I depicts the results of each grid search. From this series, the $1:7$ Earth-to-satellite period ratio provides the best performance, with a maximum visibility of approximately 9.03%. With eccentricity $e = 0$, the $1:7$ orbit strikes a good balance between range and elevation constraints. With a further grid search and gradient ascent algorithm in terms of inclination angle and semi-major axis, we find that the 1:7 orbit performs better with a deeper inclination angle of 48.5°. The resultant percent visible is 9.72%.

2) Non-harmonic orbits

The results of the grid search for high visibility circular orbits are depicted in Figure 22. The results indicate that the harmonic orbit with a semi-major axis or 11500 km gets more visibility than any nearby non-harmonic orbit, because the harmonic orbit can position its ground track precisely (see Figure 5), while the non-harmonic orbits have smeared, non-repeating ground tracks (Figure 23) reducing the visibility despite the higher altitude.

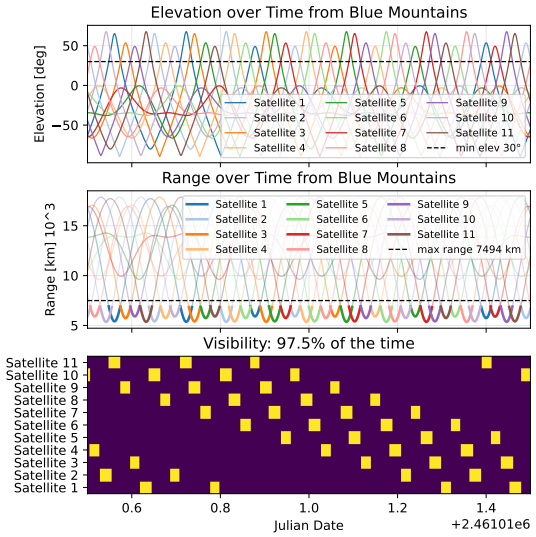

Figure 2: Elevation over time, range over time, visibility over time, and the percentage of the time at least one satellite is visible

3) Building a constellation

With a single satellite being visible for 9.9% of the time, at least 11 satellites are required for constant coverage. We can create a constellation by offsetting the phase and RAAN of each satellite such that the satellites travel equally spaced along the same ground track. True anomaly has been pushed back by $7 \times 360/11°$ to ensure each satellite passes over the ground station in the same way. This configuration is a special case of the Walker Delta configuration that only has 1 satellite per orbital plane [3]. With this configuration (Table II), we achieve over 97.5% visibility for 30° elevation, and **100% visibility for 25° of elevation**, meeting our requirements.

k	a [km]	e	i [°]	ω [°]	Definitions
0 : 10	11504	0	49	270	$\Delta\Omega = \frac{360°}{11}$, $\Omega_k = (k\,\Delta\Omega) \bmod 360°$ $\theta_k = (182° - 7k\,\Delta\Omega)\%360°$

Table II: Constellation orbital parameters (Keplerian, parameterised)

Full table is in appendix Table VIII

4) Analysis of a satellite

Because each of the satellites have the same orbital parameters, equally spaced RAAN and a true anomaly shifted to ensure that the satellites all pass over the same part of the sky, each satellite has the same ground track (see Figure 24). The first satellite, Satellite 1, was chosen arbitrarily for analysis, due to analysis being the same for each of the satellites geometrically.

The justification for each of the parameters for Satellite 1 are summarised in the list below.

- a = 11504 km: Corresponds to a 1:7 orbit period with the Earth's rotation rate, accounting for precession of RAAN

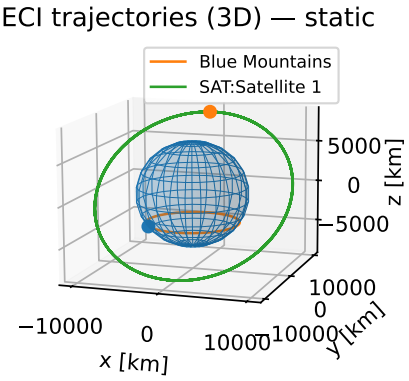

Figure 3: Orbit Trajectory of Satellite 1 Over 3.41 Hours in the ECI Frame

due to J2. Large to maximise coverage.

- e = 0: The satellite is visible at four different true anomalies, zero eccentricity (a circular orbit) ensures that the satellite is always at max altitude, increasing visibility interval duration and coverage.
- i = 49: Inclination angle equals the southern most latitude. A high inclination angle ensures some satellite passings are slightly South and others are slightly North of the Blue Mountains 5.
- Ω = 0: With a harmonic orbit, ground track position can be controlled with either TA or RAAN.
- ω = 270: With a positive inclination angle and a 270 degree AOP, the apogee passes over the northern hemisphere and the perigee passes over the southern hemisphere. This has no effect when $e = 0$.
- θ = 182: For our chosen epoch, the 1st of January 2026, this true anomaly has been optimised to align the ground track such that visibility is maximised.

5) Orbital Period and Plot

The orbital period is given by, $T = \sqrt{\frac{4\pi^2 a^3}{\mu}} = 12280$ s $=$ 3.41 hrs. This is just short of a seventh of a day (3.42 hrs). This shorter orbit counteracts the westward regression of the ascending node induced by the J2 acceleration term. The satellite's orbit in the ECI frame is depicted in Figure 3.

6) Ground Tracks

The ground track is depicted in 4. Note that the repeating ground track has been positioned around the ground station to maximise total visibility duration through the day, as seen in Figure 5. A satellite is visible when it is in figure 5's shaded blue region, imposed by the 30 degree elevation angle constraint.

It should be noted that the constellation does not have constant global coverage, but due to symmetry, has near constant and equal coverage around 14 locations spaced around the Earth (7 in the Northern Hemisphere, and 7 in the Southern) as depicted in Figure 5. This means that while satellites aren't communicating with the Blue Mountains, they can provide other locations around the world with emergency communications.

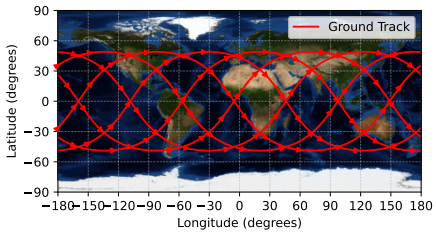

Figure 4: Ground Track of Satellite 1

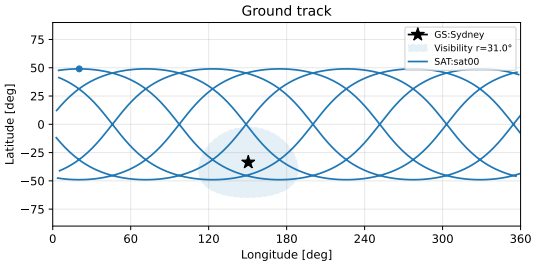

Figure 5: Ground Track of a Satellite and Visibility Region.

The satellite has four passes through each of these zones of high coverage as depicted in Appendix Figure 25. Two of them last 38.2 minutes, and the other two last 30.0 minutes, leading to a total communication time per satellite of 136.4 minutes. These intervals provide long periods of uninterrupted reliable communication and infrequent switching between satellites on short time scales.

The maximum revisit time for the Satellite 1 is 12.0 hours, which occurs while the ground station's LST points away from the low latitude part of the satellite's orbit. During this time the satellite can facilitate communication with other sites around the world. The minimum revisit time is 3.17 hours, corresponding to the two satellite passings due south of the ground station ocurring one orbit period apart.

The minimum and maxmium slant ranges to the Blue Mountains are 5418 and 6890 km respectively. This corresponds to a latency range of $\frac{[5418,6890]}{3\times10^2} = [18.1, 23.0]$ ms. The total round trip time will be less than 50 ms, which is faster than human reaction time.

7) Conclusion

By constructing an 11-satellite Walker Delta-style constellation in the $1:7$ orbit, phase-shifted in RAAN and true anomaly, we achieve continuous coverage of the Blue Mountains ground station with over 97% visibility at 30° elevation and full coverage at 25°. Each satellite provides long communication intervals with low switching frequency, acceptable revisit times, and latencies below human perceptual thresholds.

Although the constellation does not guarantee global coverage, its symmetry ensures that at least 14 equally distributed regions worldwide also benefit from near-continuous visibility. This makes the configuration robust communication with emergency services in the Blue Mountains, but also other local areas around the world.

II. Question 2

A. Introduction

Although our satellite constellation will ensure constant communication in the short term, it is important the a ground station be set up for monitoring the orbits of the satellites, so that adjustments can be made to the orbits and/or communication infrastructure after launch.

Without orbit determination from a ground station satellites must be responsible for maintaining their own orbits, which may require a GNSS receiver, Earth horizon tracking, ranging, star/tracking, and precise IMUs. It is because of cost and reliability that ground base systems are the traditional, proven choice for orbit determination [4].

This section will explore three major methods of orbit determination: Gibbs' Method, Lambert's Method, and Gauss's Method. Each method will be assessed by how they handle measurement imprecision, and what this means in the context of our mission. Then we will explore different sources of noise, and discuss their impacts on each of the three methods. Finally, an orbit determination method will be selected.

B. Method

1) Ground Station Selection

The Ground Station for satellite tracking was chosen to be Newcastle, due to its proximity to Sydney and the Blue Mountains, and its good visibility with the sky due to a flat topography. Newcastle is at the Pacific Ocean, giving it a low horizon in the north, east, and south directions.

2) Calculating Range, Azimuth, and Elevation

If we have the coordinates of our satellites in the ECI frame, and the ground station in ECI (explored in Section I-B2), we can find the vector of the satellite relative to the ground station in the ECI frame $\boldsymbol{\rho}_{ECI}$. Then we follow the procedure from Section I-B4 which involves the equation,

$$\boldsymbol{\rho}_{ENU} = \boldsymbol{Q}_{Xx}\ \boldsymbol{\rho}_{ECI}$$

where $\boldsymbol{Q}_{Xx}$ is the transformation matrix to the ENU frame defined in Equation 5.

Azimuth and Elevation are then calculated with Equations 7 and 8. Range can simply be calculated as the magnitude of the displacement vector.

$$\rho = |\boldsymbol{\rho}_{ENU}|$$

The results for our chosen satellite and new ground station are depicted in Section II-C.

3) Finding Maximum Elevation and Visibility Percentage

The maximum elevation can be found by performing the above ECI to azimuth, elevation, and range for each state in the state array (see Section I-B1), then selecting the largest value.

If each sample in the state array is a constant time apart, the visibility percentage $p_{visible}$ can be calculated with,

$$p_{visible} = \frac{n_{visible}}{n_{samples}} \times 100$$

Where $n_{visible}$ and n_{states} are the number of visible and number of total samples in the state array. $n_{visible}$ is given by,

$$n_{visible} = |i|$$

where

$$\{i \subseteq S : \alpha_i > 30\ \wedge\ r_i < 7498\}$$

where S is the set of all samples $\{1, 2, 3, ...n_{samples}\}$ each with azimuth, elevation and range A_i, α_i, r_i.

4) Simulating SLR

Satellite Laser Ranging (SLR) is a technique used to measure the distance of satellites in orbit. It involves sending a laser pulse, which bounces off retroreflectors on a satellite, and uses time-of-flight to estimate distance. The technique uses ephemeris data, and/or optical telescopes for pointing in the correct direction.

The SLR system has been modelled as a sensor that obtains the azimuth, elevation, and range of a satellite at a given time. This is implemented by taking the samples from set S that correspond to the observation times of the SLR sensor.

Gibbs' method requires three positional vectors of the satellite in the ECI frame. We do the inverse process of what was outlined in Section I-B4. To convert from azimuth, elevation and range to ECI, we first convert to ENU.

$$\rho_{ENU,x} = |\boldsymbol{\rho}| \cos(\alpha) \sin(A)$$

$$\rho_{ENU,y} = |\boldsymbol{\rho}| \cos(\alpha) \cos(A)$$

$$\rho_{ENU,z} = |\boldsymbol{\rho}| \sin(\alpha)$$

Then we calculate the line of sight vector in ECI with,

$$\boldsymbol{\rho}_{ECI} = \boldsymbol{Q}_{xX}\ \boldsymbol{\rho}_{ENU} \tag{9}$$

where

$$\boldsymbol{Q}_{xX} = \boldsymbol{Q}_{Xx}^T$$

with $\boldsymbol{Q}_{Xx}$ defined in Equation 5.

Lastly, we can calculate our position vector $\boldsymbol{r}_{ECI}$ with,

$$\boldsymbol{r}_{ECI} = \boldsymbol{\rho}_{ECI} + \boldsymbol{R}_{ECI}$$

where $\boldsymbol{R}_{ECI}$ is obtained from LLA by a process outlined in Section I-B2. After this step, our observation data is ready for Gibbs' algorithm.

5) Simulating a Radiometric Tracker

Similarly to SLR, Radiometric Tracking utilises two-way time-of-flight of a signal to calculate distance from a ground station. The setup typically involves a radio transmitter and receiver at the ground station and a transponder on the target satellite.

The radio wave beam is typically very narrow. For example, DSS43 in Canberra has a beam width of $0.0038°$ [5]. For this reason, satellite ephemerides are also required. Although velocity information can also be obtained through Doppler analysis our model captures only azimuth, elevation, range and time observations $(A_i, \alpha_i, r_i, t_i)$.

Lambert's method requires two positional vectors of the satellite, and a time difference $\Delta t = t_2 - t_1$ between the observations. In a similar fashion to the previous section (Section II-B4), we can find our satellite position vectors $\boldsymbol{r}_{ECI}$. Then we would be ready for applying Lambert's method.

6) Simulating an Optical Tracker

Optical tracking systems use optical telescopes to locate the angular position of a target satellite in a wider field of view than that of radio telescopes. For this reason, they require less a priori information, but have the shortcoming of not giving range information. Our optical tracking sensor model takes azimuth elevation observations A_i, α_i at time t_i.

Gauss' method requires three line of sight direction cosine vectors (in ECI), three ground station position vectors (in ECI) and three observation times t_1, t_2, t_3.

To find the direction cosines of the line of sight vectors, we follow a similar process outlined in Section II-B4, but this time we aren't concerned with $|\boldsymbol{r}|$. Let $\hat{\boldsymbol{\rho}}$ be the direction cosine of $\boldsymbol{\rho}$. Therefore,

$$\hat{\rho}_{ENU,x} = \cos(\alpha)\sin(A)$$
$$\hat{\rho}_{ENU,y} = \cos(\alpha)\cos(A)$$
$$\hat{\rho}_{ENU,z} = \sin(\alpha)$$

Using Equation 9 we can find $\hat{\boldsymbol{\rho}}_{ECI}$.

The ground station positions $\boldsymbol{R}_{ECI}$ are obtained from LLA by the process outlined in Section I-B2. With $\hat{\boldsymbol{\rho}}_{ECI_i}, R_{ECI_i}, t_i$ for $i \in 1, 2, 3$, we can readily perform Gauss' method.

7) Gibbs' Method

Gibbs' method of preliminary orbit determination begins with our ECI position vectors,

$$\boldsymbol{r}_1, \boldsymbol{r}_2, \boldsymbol{r}_3$$

We calculate their magnitudes,

$$r_i = |\boldsymbol{r}_i|$$

We calculate intermediate values N, D, S,

$$N = r_1(\boldsymbol{r_2} \times \boldsymbol{r_3}) + r_2(\boldsymbol{r_3} \times \boldsymbol{r_1}) + r_3(\boldsymbol{r_1} \times \boldsymbol{r_2})$$
$$D = (\boldsymbol{r_1} \times \boldsymbol{r_2}) + (\boldsymbol{r_2} \times \boldsymbol{r_3}) + (\boldsymbol{r_3} \times \boldsymbol{r_1})$$
$$S = \boldsymbol{r}_1(r_2 - r_3) + \boldsymbol{r}_2(r_3 - r_1) + \boldsymbol{r}_3(r_1 - r_2)$$

Gibbs' method assume the three observations are coplanar due to orbits being lanar, we can validate this assumption by checking that,

$$\frac{\boldsymbol{r}_1}{r_1}\frac{\boldsymbol{r}_2 \times \boldsymbol{r}_3}{|\boldsymbol{r}_2 \times \boldsymbol{r}_3|} \leq 0.1$$

We also use,

$$N = |\boldsymbol{N}|$$
$$D = |\boldsymbol{D}|$$

We can calculate the velocities $\boldsymbol{v}_1, \boldsymbol{v}_2, \boldsymbol{v}_3$ at t_1, t_2, t_3 with the equation,

$$\boldsymbol{v_i} = \sqrt{\frac{\mu}{ND}}\left(\frac{\boldsymbol{D} \times \boldsymbol{r}_i}{r_i} + \boldsymbol{S}\right)$$

8) Lambert's Method

Lambert's method of orbit determination begins with ECI position vectors obtained through two ranging observations of the satellite,

$$\boldsymbol{r_1}, \boldsymbol{r_2}$$

and the time between the observations occurring dt.

The algorithm involves calculating the magnitudes,

$$r_1 = |\boldsymbol{r}_1|$$

$$r_2 = |\boldsymbol{r}_2|$$

The change in true anomaly can be calculated with,

$$\Delta\theta = \begin{cases} \cos^{-1}\left(\dfrac{\mathbf{r}_1 \cdot \mathbf{r}_2}{r_1 r_2}\right), & \text{if } (\mathbf{r}_1 \times \mathbf{r}_2)_z \geq 0 \\ 360^\circ - \cos^{-1}\left(\dfrac{\mathbf{r}_1 \cdot \mathbf{r}_2}{r_1 r_2}\right), & \text{if } (\mathbf{r}_1 \times \mathbf{r}_2)_z < 0 \end{cases} \quad \text{prograde}$$

$$\Delta\theta = \begin{cases} \cos^{-1}\left(\dfrac{\mathbf{r}_1 \cdot \mathbf{r}_2}{r_1 r_2}\right), & \text{if } (\mathbf{r}_1 \times \mathbf{r}_2)_z < 0 \\ 360^\circ - \cos^{-1}\left(\dfrac{\mathbf{r}_1 \cdot \mathbf{r}_2}{r_1 r_2}\right), & \text{if } (\mathbf{r}_1 \times \mathbf{r}_2)_z \geq 0 \end{cases} \quad \text{retrograde}$$

An orbit is prograde if its inclination angle i is $0^\circ \leq i \leq 90^\circ$. For observations $\boldsymbol{r}_1, \boldsymbol{r}_2$ less than 180° θ apart, the orbit is pro-grade if $\boldsymbol{r}_1 \times \boldsymbol{r}_2$ is positive in the z direction.

Intermediate value A is calculated with,

$$A = \sin\Delta\theta\sqrt{\frac{r_1 r_2}{1 - \cos\Delta\theta}}$$

We define,

$$y(z) = r_1 + r_2 + A\frac{zS(z) - 1}{\sqrt{C(z)}}$$

Where $S(z)$ and $C(z)$ are the Stumpff functions defined as follows,

$$S(z) = \begin{cases} \dfrac{\sqrt{z} - \sin\sqrt{z}}{(\sqrt{z})^3}, & z > 0 \\ \dfrac{\sinh\sqrt{-z} - \sqrt{-z}}{(\sqrt{-z})^3}, & z < 0 \quad (z = \alpha\chi^2) \\ \dfrac{1}{6}, & z = 0 \end{cases}$$

$$C(z) = \begin{cases} \dfrac{1 - \cos\sqrt{z}}{z}, & z > 0 \\ \dfrac{\cosh\sqrt{-z} - 1}{-z}, & z < 0 \quad (z = \alpha\chi^2) \\ \dfrac{1}{2}, & z = 0 \end{cases}$$

We can calculate our Legrange coefficients with $y(z)$. This requires knowing the universal parameter z, which corresponds to one of the roots of the equation.

$$F(z) = \left[\frac{y(z)}{C(z)}\right]^{\frac{3}{2}} S(z) + A\sqrt{y(z)} - \sqrt{\mu}\Delta t$$

We use Newton's iterative method to find the correct root of $F(z)$. This requires $F'(z)$, given by,

$$F'(z) = \begin{cases} \left[\frac{y(z)}{C(z)}\right]^{\frac{3}{2}} \left\{\frac{1}{2z}\left[C(z) - \frac{3}{2}\frac{S(z)}{C(z)}\right] + \frac{3\,S(z)^2}{4\,C(z)}\right\} \\ \quad + \frac{A}{8}\left[3\frac{S(z)}{C(z)}\sqrt{y(z)} + A\sqrt{\frac{C(z)}{y(z)}}\right], & z \neq \\ \\ \frac{\sqrt{2}}{40}\,y(0)^{\frac{3}{2}} + \frac{A}{8}\left[\sqrt{y(0)} + A\sqrt{\frac{1}{2y(0)}}\right], & z = \end{cases}$$

With starting value $z_0 = 0$, we iteratively apply,

$$z_{i+1} = z_i - \frac{F(z_i)}{F'(z_i)}$$

Until $\frac{F(z_i)}{F'(z_i)}$ is smaller than a threshold value.

With the universal parameter z, we can find $y(z)$ and the Legrange functions $f, g, \dot{g}$ given by,

$$f = 1 - \frac{y(z)}{r_1}C(z) \tag{10}$$

$$g = A\sqrt{\frac{y(z)}{\mu}} \tag{11}$$

$$\dot{g} = 1 - \frac{y(z)}{r_2}C(z) \tag{12}$$

With the Legrange parameters, we can calculate $\boldsymbol{v_1}$ and $\boldsymbol{v_2}$ with,

$$\boldsymbol{v}_1 = \frac{1}{g}(\boldsymbol{r}_2 - f\boldsymbol{r}_1)$$

$$\boldsymbol{v}_2 = \frac{1}{g}(\dot{g}\boldsymbol{r}_2 - \boldsymbol{r}_1)$$

With the states fully defined at times t_1, t_2, we can go on to propagate to future states numerically, or analytically compute the Keplerian parameters.

9) Gauss's Method

If we have three observations of a satellite (as depicted in Figure 6), where the direction of ρ is known but not the magnitude, Gauss' method is the only method out of the three (Gibbs, Lambert, and Gauss) that can be used. The method takes the three direction cosine vectors $\hat{\boldsymbol{\rho}}_1, \hat{\boldsymbol{\rho}}_2, \hat{\boldsymbol{\rho}}_3$, the ground station's position at each of these observations $\boldsymbol{R}_1, \boldsymbol{R}_2, \boldsymbol{R}_3$, and the times of each of the observations t_1, t_2, t_3. The method produces a state vector $[\boldsymbol{r}_2, \boldsymbol{v}_2]$, which can then be converted analytically to Keplerian parameters.

The intervals between observations are represented by

$$\tau_1 = t_1 - t_2, \quad \tau_3 = t_3 - t_2$$

The cross products of each of the direction cosines are calculated,

$$\boldsymbol{p}_1 = \hat{\boldsymbol{\rho}}_2 \times \hat{\boldsymbol{\rho}}_3$$

$$\boldsymbol{p}_2 = \hat{\boldsymbol{\rho}}_1 \times \hat{\boldsymbol{\rho}}_3$$

$$\boldsymbol{p}_3 = \hat{\boldsymbol{\rho}}_1 \times \hat{\boldsymbol{\rho}}_2$$

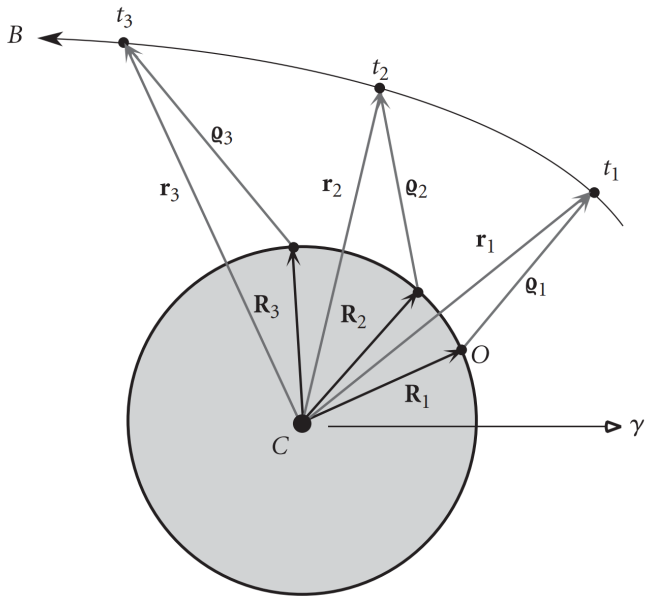

Figure 6: Illustration of vectors used by Orbit Determination Methods

Let D_0 be the scalar triple product of the direction cosines,

$$D_0 = \hat{\boldsymbol{\rho}}_1 \cdot \boldsymbol{p}_1$$

Gauss' method fails when the $\boldsymbol{\rho}$ vectors are all coplanar. If $D_0 \approx 0$, Gauss will not work well. We compute the nine scalar quantities,

$$\begin{aligned} D_{11} &= \mathbf{R}_1 \cdot \mathbf{p}_1 & D_{12} &= \mathbf{R}_1 \cdot \mathbf{p}_2 & D_{13} &= \mathbf{R}_1 \cdot \mathbf{p}_3 \\ D_{21} &= \mathbf{R}_2 \cdot \mathbf{p}_1 & D_{22} &= \mathbf{R}_2 \cdot \mathbf{p}_2 & D_{23} &= \mathbf{R}_2 \cdot \mathbf{p}_3 \\ D_{31} &= \mathbf{R}_3 \cdot \mathbf{p}_1 & D_{32} &= \mathbf{R}_3 \cdot \mathbf{p}_2 & D_{33} &= \mathbf{R}_3 \cdot \mathbf{p}_3 \end{aligned}$$

Values A, B and E are calculated with the following,

$$A = \frac{1}{D_0}\left(-D_{12}\,\frac{\tau_3}{\tau} + D_{22} + D_{32}\,\frac{\tau_1}{\tau}\right)$$

$$B = \frac{1}{6D_0}\left[D_{12}\left(\tau_3^2 - \tau^2\right)\frac{\tau_3}{\tau} + D_{32}\left(\tau^2 - \tau_1^2\right)\frac{\tau_1}{\tau}\right]$$

$$E = \boldsymbol{R}_2 \cdot \hat{\boldsymbol{\rho}}_2$$

The magnitude of the satellite's position vector at the 2nd observation, $r_2 = |\boldsymbol{r}_2|$ can be approximated by solving an 8th order polynomial,

$$F(x) = x^8 + ax^6 + bx^3 + c = 0$$

Where $x = r_2$, and the coefficients are,

$$a = -(A^2 + 2AE + R_2^2) \quad b = -2\mu B(A + E) \quad c = -\mu^2 B^2$$

Similarly to the previous section, we use Newton's method to iteratively solve for the largest real root of the polynomial.

$$x_{i+1} = x_i - \frac{F(x_i)}{F'(x_i)}$$

Where

$$F'(x) = 8x^7 + 6ax^5 + 3bx^2$$

An initial estimate x_0 is necessary to converge onto the correct root. Since our orbit has a semi-major axis of 11504 km, we choose $x_0 = 12000$ km. From our estimate of r_2, we can calculate line of sight magnitudes ρ_1, ρ_2, ρ_3 with,

$$\rho_2 = A + \frac{\mu B}{r_2^3}$$

$$\rho_1 = \frac{1}{D_0}\left[\frac{6\left(D_{31}\frac{\tau_1}{\tau_3} + D_{21}\frac{\tau}{\tau_3}\right)r_2^3 + \mu D_{31}\left(\tau^2 - \tau_1^2\right)\frac{\tau_1}{\tau_3}}{6r_2^3 + \mu\left(\tau^2 - \tau_3^2\right)}\right] - \frac{D_{11}}{D_0}$$

$$\rho_3 = \frac{1}{D_0}\left[\frac{6\left(D_{13}\frac{\tau_3}{\tau_1} - D_{23}\frac{\tau}{\tau_1}\right)r_2^3 + \mu D_{13}\left(\tau^2 - \tau_3^2\right)\frac{\tau_3}{\tau_1}}{6r_2^3 + \mu\left(\tau^2 - \tau_3^2\right)}\right] - \frac{D_{33}}{D_0}$$

We can then find the ECI coordinates of each of the satellite positions using vector geometry,

$$\begin{aligned} \boldsymbol{r}_1 &= \boldsymbol{R}_1 + \rho_1\hat{\boldsymbol{\rho}}_1 \\ \boldsymbol{r}_2 &= \boldsymbol{R}_2 + \rho_2\hat{\boldsymbol{\rho}}_2 \\ \boldsymbol{r}_3 &= \boldsymbol{R}_3 + \rho_3\hat{\boldsymbol{\rho}}_3 \end{aligned} \tag{13}$$

To find the velocities at these distances, we use first order approximations of the Legrange functions $f, g, \dot{f}, \dot{g}$,

Then, our initial estimate for $\boldsymbol{v}_2$ can be calculated with,

$$\boldsymbol{v}_2 = \frac{1}{f_1 g_3 - f_3 g_1}(-f_3\boldsymbol{r}_1 + f_1\boldsymbol{r}_3) \tag{14}$$

10) Gauss's Method (Refining)

Now that we have an initial estimate for $\boldsymbol{r}_2$ and $\boldsymbol{v}_2$, we can begin the refining part of Gauss' method.

Calculate the magnitudes vectors $r_2 = |\boldsymbol{r}_2|$ and $v_2 = |\boldsymbol{v}_2|$.

Calculate the reciprocal of the semi-major axis $\alpha = \frac{2}{r_2} - \frac{v_2^2}{\mu}$.

Calculate the radial component of $\boldsymbol{v}_2$, $v_{r2} = \boldsymbol{v}_2 \cdot \boldsymbol{r}_2/r_2$

Use Newton's method to solve the universal Kepler's equation,

$$\sqrt{\mu}\,\tau_1 = \frac{r_2 v_{r2}}{\sqrt{\mu}}\,\chi_1^2 C(\alpha\chi_1^2) + (1 - \alpha r_2)\chi_1^3 S(\alpha\chi_1^2) + r_2\chi_1$$

$$\sqrt{\mu}\,\tau_3 = \frac{r_2 v_{r2}}{\sqrt{\mu}}\,\chi_3^2 C(\alpha\chi_3^2) + (1 - \alpha r_2)\chi_3^3 S(\alpha\chi_3^2) + r_2\chi_3$$

In this case, Newton's algorithm looks like,

$$\chi_{i+1} = \chi_i - \frac{F(\chi)}{F'(\chi)}$$

where,

$$F(\chi) = \frac{r_0 v_{r0}}{\sqrt{\mu}}\,\chi_i^2 C(z_i) + (1 - \alpha r_0)\chi_i^3 S(z_i) + r_0\chi_i - \sqrt{\mu}\,\Delta t$$

$$F'(\chi) = \frac{r_0 v_{r0}}{\sqrt{\mu}}\,\chi_i\left[1 - \alpha\chi_i^2 S(z_i)\right] + (1 - \alpha r_0)\chi_i^2 C(z_i) + r_0$$

With the resulting χ_1, χ_3, we can calculate our new Legrange coefficients with,

$$f_1 = 1 - \frac{\chi_1^2}{r_2}C(\alpha\chi_1^2) \qquad g_1 = \tau_1 - \frac{1}{\sqrt{\mu}}\chi_1^3 S(\alpha\chi_1^2)$$

$$f_3 = 1 - \frac{\chi_3^2}{r_2}C(\alpha\chi_3^2) \qquad g_3 = \tau_3 - \frac{1}{\sqrt{\mu}}\chi_3^3 S(\alpha\chi_3^2)$$

With the Legrange Coefficients, intermediate variables c_1, c_3 can be calculated with,

$$c_1 = \frac{g_3}{f_1 g_3 - f_3 g_1}$$

$$c_3 = -\frac{g_1}{f_1 g_3 - f_3 g_1}$$

From these values, our updated line-of-sight magnitudes ρ_1, ρ_2, ρ_3 can be calculated with,

$$\rho_1 = \frac{1}{D_0}\left(-D_{11} + \frac{1}{c_1}D_{21} - \frac{c_3}{c_1}D_{31}\right)$$

$$\rho_2 = \frac{1}{D_0}\left(-c_1 D_{12} + D_{22} - c_3 D_{32}\right)$$

$$\rho_3 = \frac{1}{D_0}\left(-\frac{c_1}{c_3}D_{13} + \frac{1}{c_3}D_{23} - D_{33}\right)$$

Then use Equation 13 to determine $\boldsymbol{r}_1, \boldsymbol{r}_2, \boldsymbol{r}_3$

Calculate the new estimate for $\boldsymbol{v}_2$ with Equation 14. Using the new position vectors and Legrange variables.

Repeat the refining steps until a desired precision is achieved with $\boldsymbol{r}_2$ and $\boldsymbol{v}_2$. From these parameters, the Keplerian parameters can be computed.

11) Modelling Error

Sensitivity analysis was performed on each of the orbit determination methods. We introduced three types of Gaussian error: ranging error, angular error, and temporal error. The SLR system is modelled with ranging error, the radiometric tracking system with ranging and temporal error, and the optical system with angular and temporal error.

Mathematically, each observation $\tilde{x}$ is expressed as the true value x plus a Gaussian perturbation

$$\tilde{x} = x + \varepsilon, \qquad \varepsilon \sim \mathcal{N}(0, \sigma^2),$$

where the standard deviation σ is proportional to the magnitude of the observation itself. The proportionality constants α correspond to the specified error percentages.

a) Range observations.

For a true range ρ_i, the observed range is

$$\tilde{\rho}_i = \rho_i + \varepsilon_{\rho,i}, \qquad \varepsilon_{\rho,i} \sim \mathcal{N}\left(0,\, \sigma_{\rho,i}^2\right), \quad \sigma_{\rho,i} = \alpha_\rho\,\rho_i.$$

b) Angular observations.

For an angle θ_i (azimuth or elevation),

$$\tilde{\theta}_i = \theta_i + \varepsilon_{\theta,i}, \qquad \varepsilon_{\theta,i} \sim \mathcal{N}\left(0,\, \sigma_\theta^2\right), \quad \sigma_\theta = \alpha_\theta\,\theta_i.$$

c) Temporal differences.

For a time separation Δt,

$$\widetilde{\Delta t} = \Delta t + \varepsilon_t, \qquad \varepsilon_t \sim \mathcal{N}\left(0,\, \sigma_t^2\right), \quad \sigma_t = \alpha_t\, \Delta t.$$

The three orbit determination strategies, SLR with Gibbs, Radiometric with Lambert, and Optical with Gauss, were compared for the sensitivity of their orbital parameter estimates to small errors in the observations.

Our method for revealing this relationship involves performing the three strategies with errors from 0% to 1%, specifically $\alpha \in \{0, 0.001, 0.002, ..., 0.01\}$, one thousand times for each alpha value.

We conducted four experiments each respectively simulating orbit determination with range error, angular error, temporal error, and all three types of error. We compared the Keplerian parameters obtained from the predicted state vector to the true Keplerian parameters of the satellite depicted in Table VIII in row "Satellite 1".

The percentage error for each of the predicted orbital parameters is a function of the predicted orbital parameters $\hat{a}, \hat{e}, \hat{\theta}, \hat{\Omega}, \hat{i}, \hat{\omega}$ and the true values $a, e, \theta, \Omega, i, \omega$. In the case of the semi-major axis,

$$err_{\%} = \frac{a_p - a}{a} \times 100$$

In our specific case, since the orbit is circular, argument of perigee and consequently true anomaly have no meaning and thus won't be assessed.

12) Noise Assessment

An investigation into the type of noise that can affect observations takes place in the Results section II-C. This investigation informs our final choice of orbit determination method.

C. Results and Discussion

1) Calculating Azimuth, Elevation, and Range

The azimuth, elevation and range of the satellite relative to our Newcastle ground station is depicted in Figure 7. The sky track is depicted in Figure 26.

2) Finding Maximum Elevation and Visibility Percentage

We note that the maximum range when above the required elevation is 6895 km from the ground station. The maximum elevation is 69.3°. The percentage view time is 9.6% over the 24 hour period.

The range of 6895 km corresponds to a one way communication delay of $6895/(3.00 \times 10^5) = 23.0$ ms. This is comfortably within our requirement. The maximum elevation of 69.3° implies that the satellite never gets within 20° of zenith. While this setup is suitable for line-of-sight communication, signals will always have to pass through more of Earth's atmosphere than they would need to at a higher elevation angle. Additionally, due to the low maximum elevation, the satellites would be unsuitable for the narrow field-of-view imaging required for early fire detection satellites like those in the FireSat constellation [6], or NASA's Terra Satellite [7].

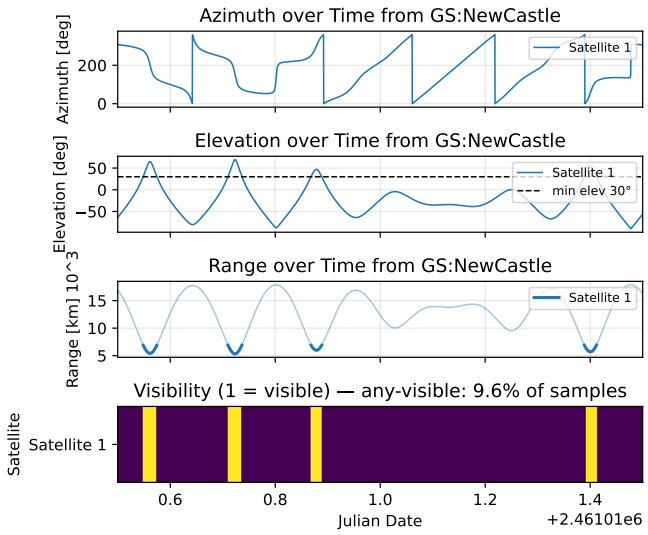

Figure 7: Azimuth, Elevation and Range over time for "Satellite 1" for one day from GS "Newcastle"

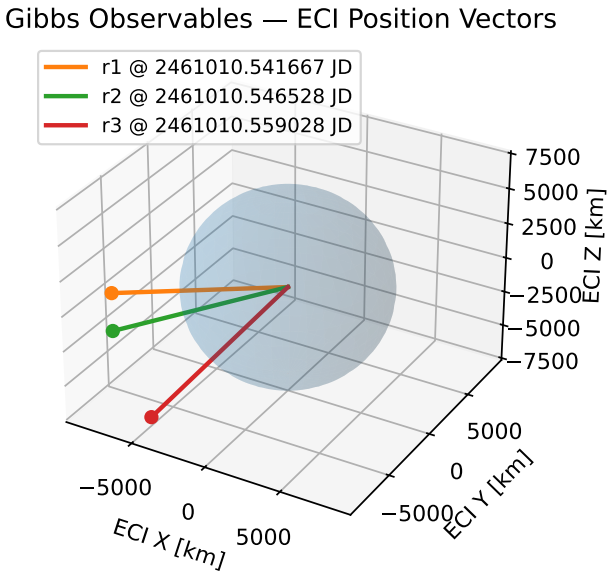

Figure 8: SLR observations of Satellite 1 at three observation times. Observations 1 and 2 also represent the radiometric tracker's observations

3) Simulating an SLR System

Our model of the SLR system observed Satellite 1 at three times. With an epoch of midday on the 1st of January 2026, the first observation time was an hour after epoch, the second was 7 minutes later, and the third was another 18 minutes later. The observations are depicted in figure 8.

The reason why the vectors come from the Earth's centre and not from the ground station coordinates is because Gibbs' method takes the satellite's position in ECI as observations. This conversion is described in the methodology, Section

II-B4. These observations are no collinear, but are coplanar, making them appropriate for Gibbs' method.

4) Simulating a Radiometric Tracker

Our radiometric tracker model provides the observations r_1 and r_2 depicted in Figure 8 as well as the time between these two measurements.

5) Simulating an Optical Tracker

Our model of the optical tracking systems made three observations of the satellite at the observation times described in Section II-B4. The observation results are depicted in Figure 9. Gauss' method performs well when the observations are in the same quarter of the orbit, and the direction cosines each lie on a different plane. The first criterion can be validated from the left subplot in Figure 6 and the second can be validated with the right graph, but also from checking that the triple scalar product 'D_0' is not close to zero (see Section II-B9).

6) Gibbs' Method

Gibbs' method produced a state vector estimate that produced an accurate reconstruction of the original orbit when propagated. The results can be seen in Figures 10 and 11.

Through inspection of these graphs, it is clear that Gibbs' method is an effective orbit determination strategy. Despite how accurate the estimate was, it is important to note how large of an effect small error has on satellite position. After a day of propagation, Gibbs' predicted satellite is over 1° East of where it should be.

For further insight, we calculate the Keplerian parameters and relative error for each parameter to produce Table III.

Table III: Error calculations for each of the relevant orbit parameters for Gibbs Method with 0% sensor error

Parameter	True	Gibbs	Absolute error	Percentage error
a [km]	11504	11505.59	1.59	0.01%
e [-]	0	0	0	N/A
i [deg]	49	49.01	0.01	0.02%
RAAN (Ω) [deg]	0	359.97	0.03	N/A

The method produced negligible error in all areas. The small error in inclination and semi-major axis may be due to J2 perturbations, which Gibbs' method does not consider, and the coarse sample rate of 10 seconds per sample producing some random error.

7) Lambert's and Gauss' Methods

Figures 12 and 13 compare the reconstructed orbits from Lambert and Gauss with the truth (Gibbs is included for reference). With 0% sensor error, all three methods reproduce the reference trajectory closely. Visually, Lambert adheres most closely to the truth over the full propagation, while Gauss shows the largest accumulated along-track separation by the end of the day-long simulation.

Quantitatively, Tables IV and V report small errors in the recovered elements. Inclination and RAAN differences are essentially negligible at about $0.01°$ and $0.03°$. The main discriminator is the semi-major axis: Lambert has a bias of 5.58 km (0.05%), while Gauss is higher at 14.73 km (0.13%). Although Gibbs shows the smallest bias in a (Table III), the Lambert solution provides the best overall trajectory agreement in Figures 12 and 13, indicating better velocity phasing for this geometry.

From a methodological perspective, Lambert uses two position vectors and the known time-of-flight, which strongly constrains the orbit. Gauss is based on angles-only data and is more sensitive to viewing geometry over short arcs, which is consistent with the larger a error in Table V.

Table IV: Lambert element errors with 0% sensor error.

Parameter	True	Lambert	Absolute error	Percentage error
a [km]	11504	11509.58	5.58	0.05%
e [-]	0	0	0	N/A
i [deg]	49	49.01	0.01	0.02%
(Ω) [deg]	0	359.97	0.03	N/A

Table V: Gauss element errors with 0% sensor error.

Parameter	True	Gauss	Absolute error	Percentage error
a [km]	11504	11518.73	14.73	0.13%
e [-]	0	0	0	N/A
i [deg]	49	49.01	0.01	0.03%
RAAN (Ω) [deg]	0	359.97	0.03	N/A

8) Sensitivity Analysis

As described in the Error Analysis Method Section II-B11, we conducted four experiments for our sensitivity analysis, with results depicted in Figure 14, 15, 16, and 17 respectively. When error is introduced, each of the three methods are affected in different amounts.

a) Range error discussion

From Figure 14, we observe that Gauss is unaffected by error in range. This is expected, as Gauss determines orbits with just angular and temporal measurements. Interestingly, while Lambert predicts the semi-major axis and eccentricity more accurately than Gibbs does, Gibbs performs better when it comes to predicting inclination and RAAN.

Lambert's relative success can be explained by the fact that Lambert's method utilises time, which in this case has no error, while Gibbs just utilises the erroneous position measurements. Lambert performs worse with inclination and RAAN, because these have no dependence on the time of observations, resulting in Lambert losing its advantage. Furthermore, since Gibbs has three independent position vectors while Lambert only has two, the resulting angular elements are predicted better as a result of less dependence on the accuracy of any one vector.

b) Angular Error discussion

From Figure 15, we notice early catastrophic failure in the performance of Gauss's method; while our true orbit is circular, Gauss's method predicts an eccentricity of 0.18 on average for 0.1% angular error, i.e. error of $0.36°$. Furthermore, Gauss's method predicts, on average, hyperbolic orbits for observation errors with a standard deviation of $1.08°$, although this may be indicative of a few catastrophic failings dominating the average eccentricity over the course of a 1000 trials. Gauss's method as a result also predict semi-major axis several times larger than the true semi-major axis.

On the other hand, Lambert and Gibbs perform well in the face of angular error, due to them leveraging ideal range

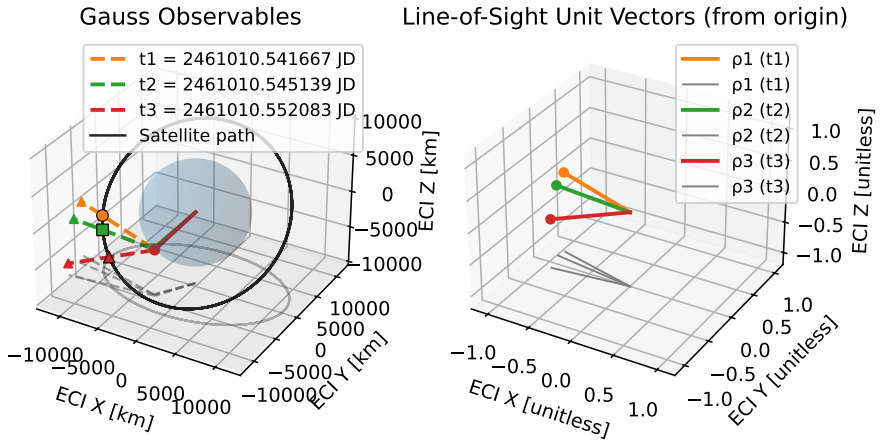

Figure 9: Optical tracker observations ready for Gauss' method. The figure on the left features the GS position, line-of-sight rays, satellite path, and Earth. The line-of-sight direction cosines are illustrated on the right.

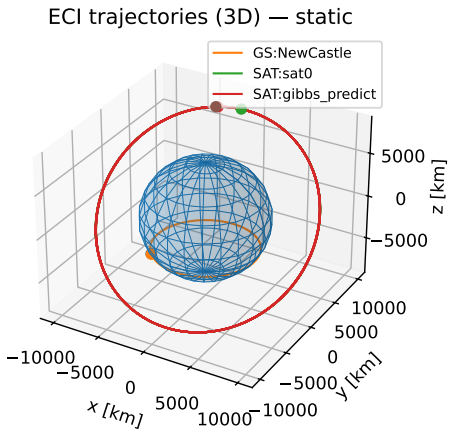

Figure 10: 3D Orbits of our satellite and a reconstructed satellite using the results of Gibbs' method.

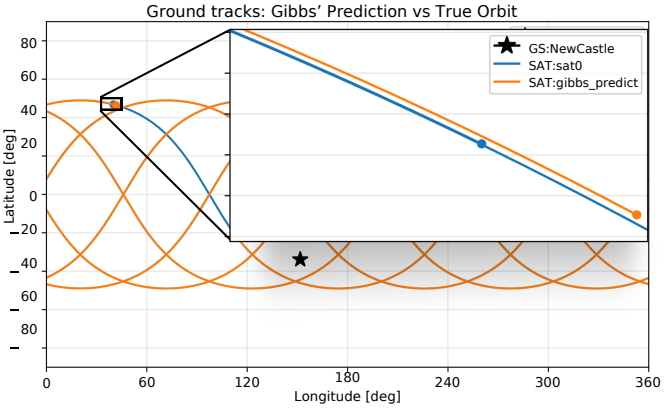

Figure 11: Ground tracks of our satellite and a reconstructed satellite using the results of Gibbs' method. The dots indicate the location of the satellite at the end of the simulation. The size of the detail window is 1° lat x 3° long.

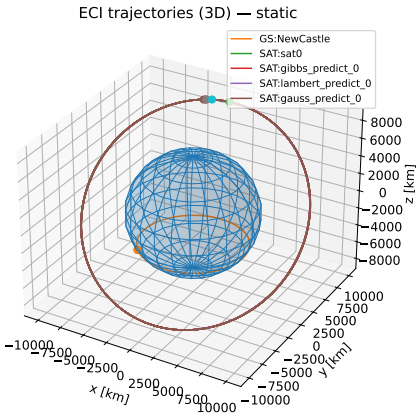

Figure 12: 3D orbits of the truth and reconstructed satellites obtained from Gibbs, Lambert and Gauss with 0% sensor error. The dots indicate the starting and ending positions of the satellites.

measurements in this case. Even with 1% error in angular measurements the absolute error in eccentricity is 0.1 for the Lambert's method, and 0.2 for Gibbs' method. The predicted semi-major axis is within 100 km for both methods. All methods are quite sensitive when it come to inclination and RAAN. For each percent increase in angular measurement error, there is $\approx 1.5 - 3\%$ increase in angular error for the predicted orbital plane. Gauss suffers the most due to its complete dependency on angular measures. Lambert performs better than Gibbs for a and e and vice versa for i and Ω for the same reasons as in the range analysis.

c) Temporal Error Discussion

From Figure 16, we observe that Gibbs' prediction accuracy is completely unaffected due to its non-reliance on time. Lambert's method performs very poorly in its a prediction for

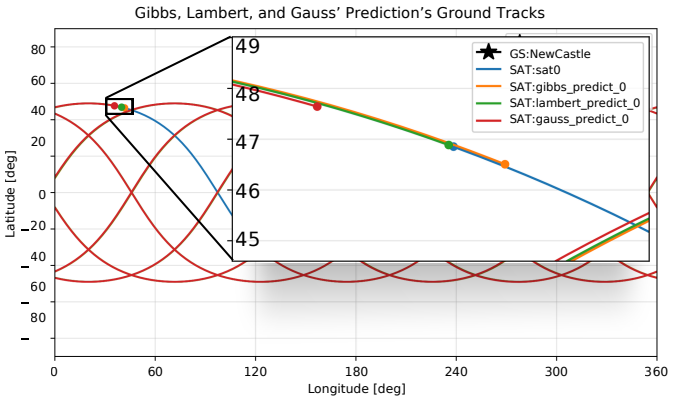

Figure 13: Ground tracks of the truth and reconstructed satellites for Gibbs, Lambert and Gauss. Dots mark final positions. The inset is $1^\circ \times 4^\circ$ and highlights small along-track offsets, smallest for Lambert and most significant for Gauss.

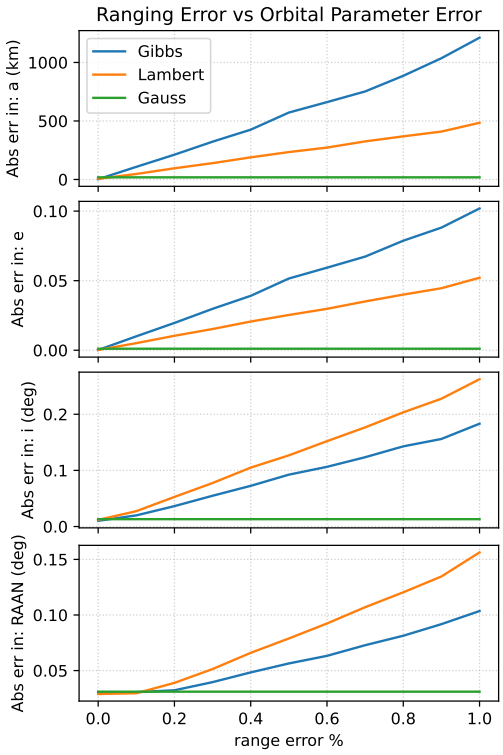

Figure 14: Average predictive accuracy for orbital parameters of the satellite with different orbital determination methods for different error magnitudes in range measurements

large temporal error because there are an unlimited number of orbits in a plane that pass through two points, and the only way to differentiate between them is with time delay. This is related to Kepler's 3rd Law. Gauss's method suffers less in this regard because it is able to estimate ranges well, only one orbit passes through three points, reducing the dependence on time.

All three methods predict the eccentricity, RAAN, and inclination within 0.01°, 0.1°, and 0.1° of a degree respectively for up to even 1% timing error. We can infer that measurement

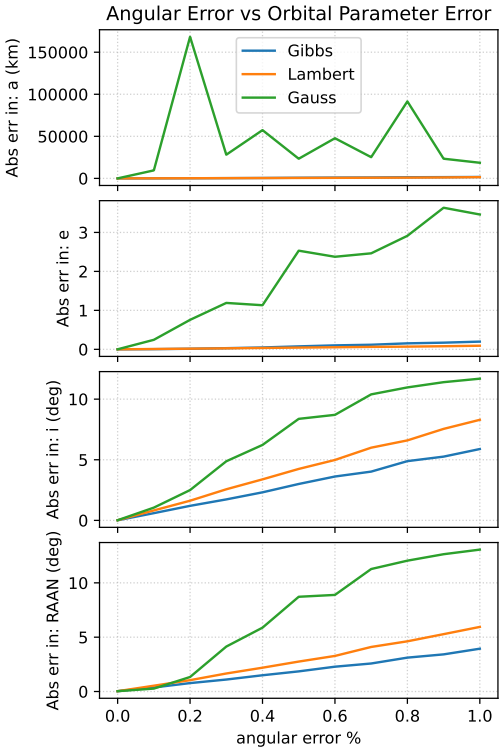

Figure 15: Average predictive accuracy for orbital parameters of the satellite with different orbital determination methods for different error magnitudes in angular measurements

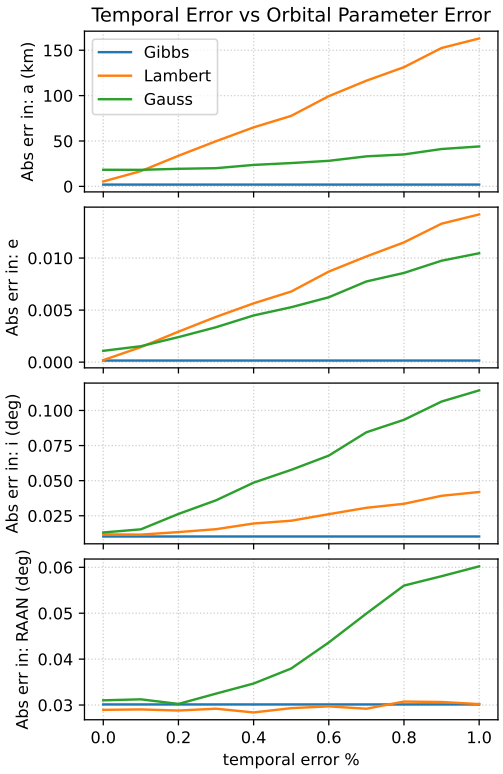

Figure 16: Average predictive accuracy for orbital parameters of the satellite with different orbital determination methods for different error magnitudes in temporal measurements

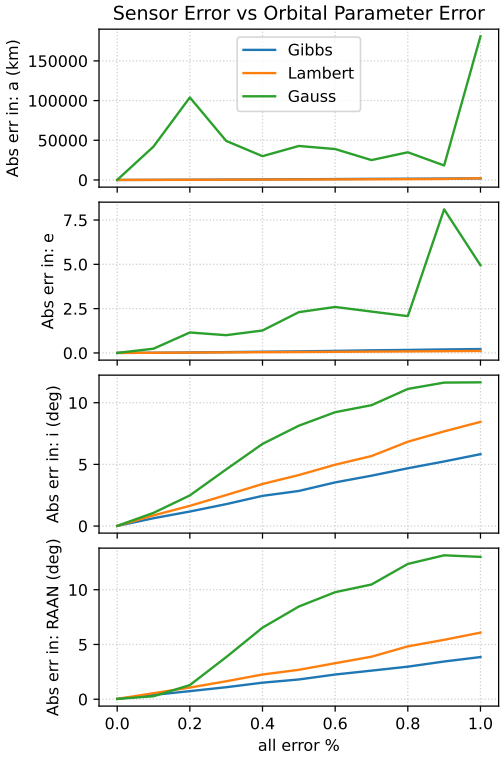

Figure 17: Average predictive accuracy for orbital parameters of the satellite with different orbital determination methods for measurement error magnitudes.

error in timing is less consequential than measurement error in range or angle.

d) All Error Discussion

When ranging, angular, and temporal measurement error is simulated simultaneously, it is clear that Gauss is the least fit for the tasks, performing the worst in each category, despite the observation conditions being appropriate for the application of Gauss's method.

Gibbs' performs worse compared to Lambert in the prediction of a and e, while Lambert performs slightly worse with i and Ω. **We select Gibbs' method as our preferred orbit determination method** due to consistently better performance with predicting the angular elements, which solely define the sky track, allowing us to know where to point for future observations, and invariance against temporal inaccuracy.

9) Noise Assessment

In practice, measurement noise and modelling errors dominate orbit determination (OD) performance. Here we summarise the principal noise sources for *Satellite Laser Ranging* (SLR), *radiometric tracking* (two-way range), and *optical tracking* then explain how these noises map into the three OD methods we evaluated (Gibbs, Lambert, Gauss).

a) Satellite Laser Ranging

SLR measures two-way time-of-flight of short laser pulses to retroreflectors, achieving millimetre-level range precision in normal points at well-calibrated sites. Dominant error terms are:

- **Timing and system calibration**: Since ranging requires measuring time-of-flight, SLR systems are very sensitive to timing imprecision. Satellite laser ranging typically involves event timers that operate on a scale of picoseconds to tens of picoseconds, resulting in sub-millimetre accuracy in theory. In practice, due to systematic error such as calibration error, the systems are generally precise to the 10s of centimetres [8]. This source produces the largest unavoidable error.
- **Tidal Atmospheric Loading**: Diurnal (S1) and semi-diurnal (S2) atmospheric pressure tides periodically deform the Earth's crust by up to 1.5 mm, [9]. When access to tidal information is unavailable, this small error can bias the distance measurement.
- **Atmospheric Refractive Effects** Depending on the frequency and observation angle, refractive effects can increase the distance estimation on the scale of metres. Fortunately, these effects are well modelled, and can be removed post-observation.
- **Target effects**: Retroreflector array geometry relative to the centre of mass of the satellite can create a bias equal to the radius of the satellite [8]. Additionally, heating can change the geometry of the satellite at the mm scale.
- **Gravitational Effects**: Ocean tides, tectonic activity, and higher order perturbation terms all affect the satellite's motion in well understood ways [9].

Impact on elements/methods: Range is the most direct constraint on orbital energy, so SLR noise primarily perturbs a. If gravitational, atmospheric, and target effects are accurately modelled, which modern systems do [8], then the noise experienced will be on the scale of centimetres, primarily due to the timing limitations of the system's electronics. If the satellite is large, then target effects may increase the noise to the order of metres.

SLR systems get angular measurements from telescope systems. The noise characteristics of these systems will be explored in the Optical Tracker section later.

Radiometric tracking (two-way range and Doppler)

Deep Space Network-style radiometrics provide two-way group delay range. Principal noises include:

- **Solar Plasma**: Solar wind and corona plasma make radio waves travel slower than they would in a vacuum. This phenomenon can cause ranging inaccuracy of up to 2.3 m, which occurs at small Sun-Earth-Probe angles [10]. This source has the largest impact on error.
- **Station Delay** Station delay is the time taken from receiving a signal to getting it to the Downlink Tracking and Telemetry (DTT) system. Station delay can cause noise on the order of tens of centimetres [10].
- **Thermal Noise**: Historically producing noise on the order of 10s of cm, thermal noise can become an issue with radiometric tracking. This can be mitigated through cooling the receivers to lower temperatures [10].

- **Satellite Transponder**: Delays in the transponder on the satellite can produce noise with a standard deviation of between millimetre and centimetre [10].

Impact on elements/methods: Gibbs and Lambert (using position vectors from radiometric solutions or radar) benefit from accurate range, facilitating more accurate e and a calculations. Gauss does not use Doppler or range and thus cannot exploit radiometric strengths. We should expect that ranging error be of the scale of metres due to the effects of Solar plasma, although some research has reduced its effects to the scale of centimetres [10].

b) Optical trackers

Optical tracking measures line-of-sight directions against the celestial sphere. The main sources of noise include

- **Motor and Encoder precision**: Due to hardware, optical telescopes cannot be pointed exactly at the target, and the exact position of the telescope cannot be known. Modern optical tracking systems, which often use direct drive permanent magnet synchronous motors has sub arc second ($0.5''$) accuracy [11]. Other common methods achieve accuracies of around $0.3''$ to $2.4''$ [12], [13], [14]. This source has the largest impact on error.
- **Target effects**: The satellite's photocentre may not align with its COM. At 7500 km, a metre difference in centres results in $1\ \mathrm{m}/7500\ \mathrm{km} \approx 0.027''$.
- **Atmospheric Effects**: Jitter in the angle of incident light described by Roddier's classic review can be a source of up to $0.3''$ error in angular readings [12].

Impact on elements/methods: Because of its importance to not just orbit determination, but also astronomy, precise pointing technology has been pushed to be able to provide measurements in the arc second range after all error is considered, facilitating accurate angular measurements for Gibbs', Lambert's and Gauss's orbit determination methods. Error in angular measurement disproportionately effect estimations for RAAN, Inclination, and AOP, because these elements do not depend on range.

10) Selection of Orbit Determination method

The sensitivity analysis described in Section II-B11 was repeated with error values corresponding to the noise characteristics of each of the sensors.

The specific noises for each of the sensors are in Table VI.

Method	Ranging σ[m]	Angular σ[arcs]	Temporal σ[ps]
Gibbs	0.03	2.0	25
Lambert	1.0	2.0	25
Gauss	0	0.6	25

Table VI: Sensor noise settings (1σ ranges) used in simulations.

The results are depicted in Table VII. From the table, we note that Lambert now performs worse than Gibbs at predicting all parameters except RAAN. In light of radiometric tracking's susceptibility to noise induced by Solar plasma, which is on the order of metres, and reliance on transponders on our target satellites, we gain further confidence in our choice of **Gibbs' method with Satellite Laser Ranging (SLR) as our chosen orbit determination method.**

Table VII: Average absolute errors over 1000 trials (rows = methods).

Method	a [km]	e [-]	i [deg]	RAAN (Ω) [deg]
Gibbs	1.72759	0.00019	0.01111	0.02945
Lambert	8.00495	0.00072	0.01213	0.02883
Gauss	14.17567	0.00079	0.01434	0.02985

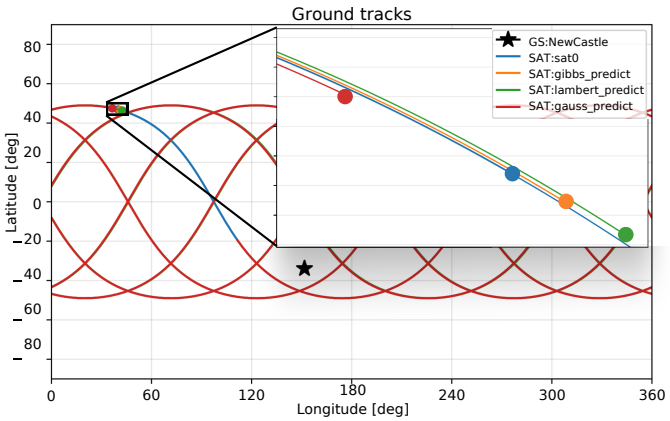

Figure 18: Ground track plots of each of the methods' predicted satellites. Gibbs' method performs the best in light of our more realistic noise model

With one of the trials, satellites were constructed from the predicted orbital parameters to produce Figure 18.

D. Conclusion

Throughout the second half of this report, a ground station, sensors, and an orbit determination technique were chosen for tracking the satellite constellation that was designed in the first half of the report.

Newcastle was selected to be our ground station. Due to its proximity to the sea, it has low horizons over which satellites can easily be spotted.

Three different sensor systems were statistically modelled, the Satellite Laser Ranger (SLR), radiometric tracker, and optical telescope. Observations from their sensors were used for the Gibbs, Lambert, and Gauss orbit determination techniques respectively.

A sensitivity analysis was performed to understand how robust each of these pairing were in the face of synthetic error. Gibbs' method proved the most robust, due to its better performance in predicting angular measurements such as RAAN and inclination angle in the face of high error when compared to Lambert's and Gauss's methods. Furthermore Gibbs' method was independent of any timing error.

Our noise model further highlighted the benefits of SLR. The shorter wavelengths of optical laser systems are less affected by the Solar plasma than the long wavelength radio wave used in radiometric tracking. We found that SLR systems were more precise, resulting in better orbit determination by almost every metric compared to the other two.

III. Appendix

A. Question 1

Table VIII: Constellation orbital parameters (Keplerian)

Key	a [km]	e	i [°]	RAAN [°]	AOP [°]	TA [°]
Satellite 1	11504	0	49	0	270	182
Satellite 2	11504	0	49	33	270	313
Satellite 3	11504	0	49	65	270	84
Satellite 4	11504	0	49	98	270	215
Satellite 5	11504	0	49	131	270	346
Satellite 6	11504	0	49	164	270	117
Satellite 7	11504	0	49	196	270	247
Satellite 8	11504	0	49	229	270	18
Satellite 9	11504	0	49	262	270	149
Satellite 10	11504	0	49	295	270	280
Satellite 11	11504	0	49	327	270	51

B. Question 2

References

[1] Australian Space Agency, "Australia's emergency services rely on space." https://www.space.gov.au/Australian-emergency-services-rely-on-space, 2025. Accessed 17 August 2025.

[2] "Application for fixed satellite service by space exploration holdings, llc." FCC Filing SAT-MOD-20181108-00083 / SATMOD2018110800083, Nov. 2018. Archived from the original on November 17, 2020. Retrieved March 24, 2019. Public Domain.

[3] J. G. Walker, "Circular orbit patterns providing continuous whole earth coverage," RAE Technical Report 70211, Royal Aircraft Establishment, Farnborough, UK, 1970. Original report introducing Walker satellite constellation patterns.

[4] M. R. Ackermann, R. R. Kiziah, P. C. Zimmer, J. T. McGraw, and D. D. Cox, "A systematic examination of ground-based and space-based approaches to optical detection and tracking of satellites," in *31st Space Symposium, Technical Track*, (Colorado Springs, CO, USA), Apr. 2015. Ground-based radar is traditionally used for detection and tracking of space objects in LEO, and optical systems are necessary for MEO and GEO tracking.

[5] W. D. Jones, "50 years later, this apollo-era antenna still talks to voyager 2," Apr. 2024. IEEE Spectrum. Willie Jones covers transportation for IEEE Spectrum and the history of technology for The Institute.

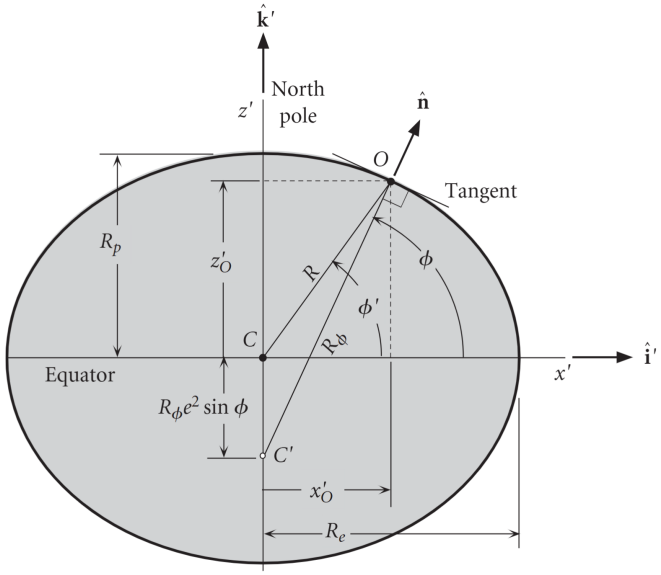

Figure 19: The relationship between geocentric latitude (ϕ') and geodetic latitude (ϕ), source: [15]

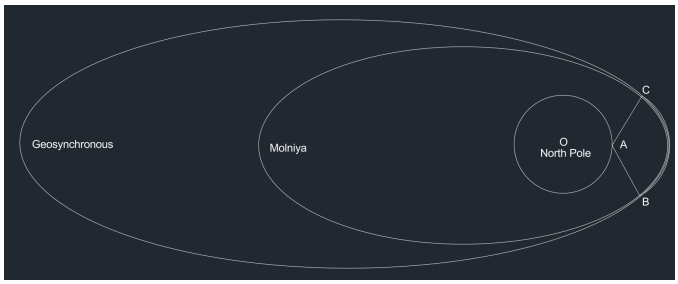

Figure 20: Tundra and Molniya orbits

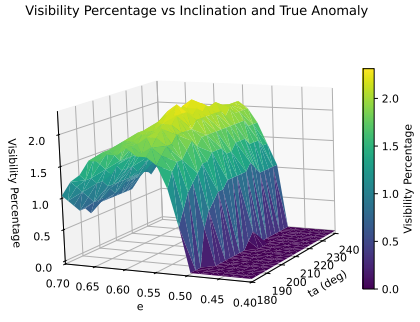

Figure 21: Communication time as a percentage of orbital period as a function of true anomaly and eccentricity for a Molniya-like orbit

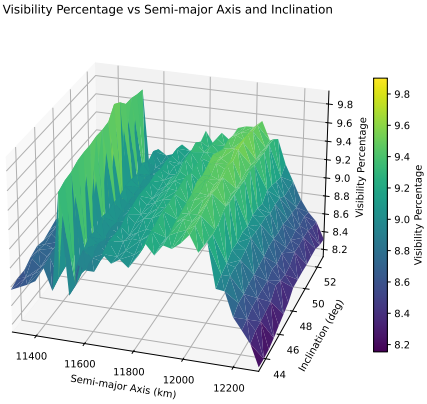

Figure 22: Grid search for the highest visibility as a function of semi-major axis and inclination angle over simulation duration of 20 days. The sharp ridge is the 1:7 harmonic orbit, which is achieving 9.9 percent visibility

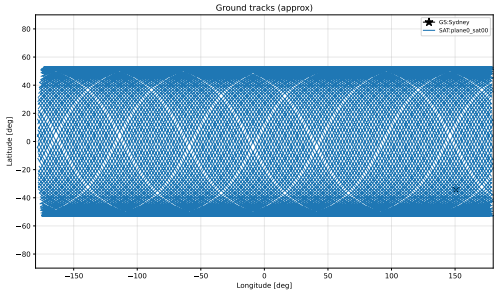

Figure 23: Ground Track of non harmonic orbit over the course of a week

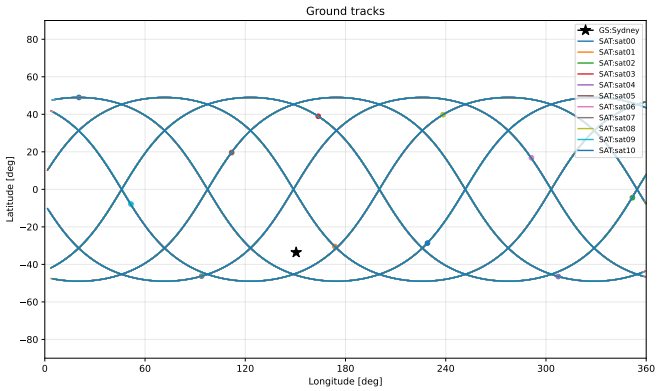

Figure 24: Ground tracks of chosen constellation

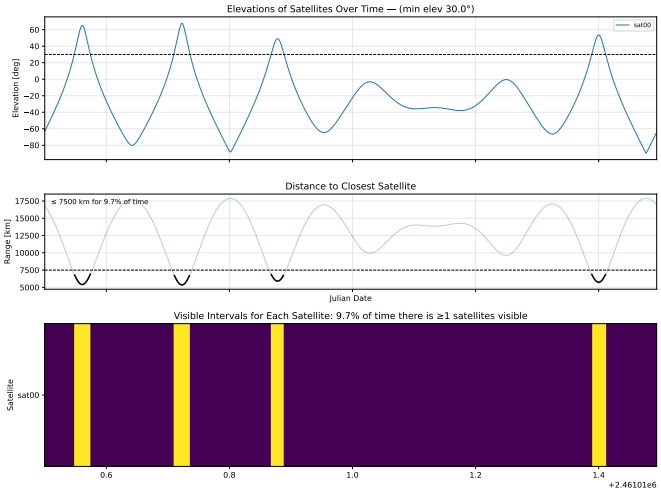

Figure 25: Elevation, distance, and visibility of Satellite 1 over time

[6] J. S. Levine, ed., *Biomass Burning and Global Change. Volume 1: Remote Sensing, Modeling, and Inventory Development*. Cambridge, MA: MIT Press, 1996.

[7] D. P. Edwards, L. K. Emmons, D. A. Hauglustaine, D. A. Chu, J. C. Gille, Y. J. Kaufman, G. Pétron, L. N. Yurganov, L. Giglio, M. N. Deeter, V. Yudin, D. C. Ziskin, J. Warner, J.-F. Lamarque, G. L. Francis, S. P. Ho, D. Mao, J. Chen, E. I. Grechko, and J. R. Drummond, "Observations of carbon monoxide and aerosols from the terra satellite: Northern hemisphere variability," *Journal of Geophysical Research: Atmospheres*, vol. 109, no. D24, 2004.

[8] G. Appleby, J. Rodríguez, and Z. Altamimi, "Assessment of the accuracy of global geodetic satellite laser ranging observations and estimated impact on itrf scale: estimation of systematic errors in lageos observations 1993–2014," *Journal of Geodesy*, vol. 90, no. 12, pp. 1371–1388, 2016.

[9] Z. Li, W. Chen, W. Jiang, L. Deng, and R. Yang, "The magnitude of diurnal/semidiurnal atmospheric tides (s1/s2) and their impacts on the continuous gps coordinate time series," *Remote Sensing*, vol. 10, no. 7, 2018.

[10] M. Paik, J. S. Border, S. Esterhuizen, and D. K. Shin, "Advanced ranging instrumentation," *The Interplanetary Network Progress Report*, vol. 42-215, pp. 1–13, Nov. 2018. Jet Propulsion Laboratory, California Institute of Technology.

[11] T. Riel, A. Galffy, G. Janisch, D. Wertjanz, A. Sinn, C. Schwaer, and G. Schitter, "High performance motion control for optical satellite tracking systems," *Advances in Space Research*, vol. 65, no. 5, pp. 1333–1343, 2020.

[12] C. H. Park, Y. S. Son, B. I. Kim, S. Y. Ham, S. W. Lee, and H. C. Lim, "Design of tracking mount and controller for mobile satellite laser ranging system," *Advances in Space Research*, vol. 49, no. 1, pp. 177–184, 2012.

[13] Z.-P. Zhang, F.-M. Yang, H.-F. Zhang, Z.-B. Wu, J.-P. Chen, P. Li, and W.-D. Meng, "The use of laser ranging to measure space debris," *Research in Astronomy and Astrophysics*, vol. 12, no. 2, pp. 212–218, 2012.

[14] K. Riesing, H.-S. Yoon, and K. Cahoy, "A portable optical ground station for low-earth orbit satellite communications," in *2017 IEEE International Conference on Space Optical Systems and Applications (ICSOS)*, pp. 1–7, IEEE, 2017.

[15] H. D. Curtis, *Orbital Mechanics for Engineering Students*. Elsevier / Butterworth-Heinemann, 3rd ed., 2013.

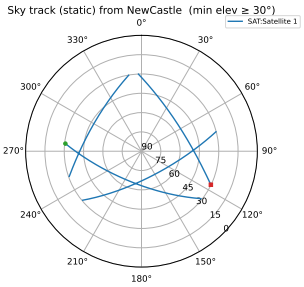

Figure 26: Sky track of Satellite 1 over a period of 1 day